

Changing the properties of $\text{Hf}_{0.5}\text{Zr}_{0.5}\text{O}_2$ during cyclic repolarization of ferroelectric capacitors with different electrode materials

Timur M. Zalyalov^{1,2, a)} and Damir R. Islamov^{1,2}

¹⁾*Rzhanov Institute of Semiconductor Physics, Siberian Branch of the Russian Academy of Sciences, Novosibirsk 630090, Russian Federation*

²⁾*Novosibirsk State University, Novosibirsk 630090, Russian Federation*

(Dated: 9 August 2024)

The interest in the ferroelectric non-volatile memory as a candidate for low power consumption electronic memories was raised after the discovery of ferroelectricity in hafnium oxide. Doping by different elements of hafnia films allows improving their ferroelectric properties. In this work, the transport experiments are combined with the simulations to study the evolution of ferroelectric properties and the mean distance between oxygen vacancies during the endurance of hafnium-zirconium oxide in metal-ferroelectric-metal structures to study the impact of different metal electrodes.

PACS numbers: 72.20.Jv, 77.55.df, 77.84.Bw, 73.50.-h, 72.80.-r, 85.50.Gk

Keywords: hafnia, ferroelectrics, oxygen vacancy, leakage current, metal electrodes

The development of memory devices for using them in mobile systems, Internet-of-Things technology and in other devices with high autonomy requires non-volatile energy efficiency and high operation speed from used memory elements. One of the candidates for the role of such memory is Ferroelectric Random Access Memory (FRAM). From the last decade of the last century to the present day, FRAM elements used in microelectronics are based on lead zirconate-titanate (PZT)¹. The problem of this material is the rapid disappearance of the ferroelectric response of a PZT film with a reduction in its thickness less than 100 nm. This limitation made the FRAM production process technology to be unscalable beyond the 130 nm CMOS technology (chips manufactured by Texas Instruments), and, as a result, to a small information volume of integrated circuits. Therefore, modern research in the field of FRAM technology is focused on studying the ferroelectric properties of doped hafnium oxide HfO_2 thin films. The history of ferroelectric HfO_2 began in 2007, when the group members at the Dynamic Random Access Memory (DRAM) company Qimonda, together with the RWTH Aachen, searched for materials for DRAM capacitor applications and unexpectedly discovered the ferroelectric properties of doped thin HfO_2 films. It was demonstrated that the non-centrosymmetric polar orthorhombic phase (o-phase) between the monoclinic (m-) and tetragonal (t-) phase grains in thin (5–50 nm) doped HfO_2 layers is responsible for maintaining polarization after the external electric field is turned off^{2–4}. The HfO_2 -based FRAM technology demonstrates non-volatility, high information volume per die, high operation speed and is compatible with the modern CMOS technology⁵.

For more than 10 years, researchers were working to solve problems that prevent the implementation of HfO_2 -based FRAM devices into mass-market production. The

main problems include a small memory window ($\text{MW} = 2P_r$, double value of the remnant polarization), a small memory cell resource and instability of the memory window during cyclic repolarization of ferroelectric. A small memory window prevents a reliable reading logical state of the memory cell. A small memory cell resource (endurance) is little information rewriting cycles before the memory cell fails (breakdown). The MW instability during the cycling consists in an increase in MW at the beginning of cycling (wake-up effect) and a decrease in the memory window before a breakdown (fatigue effect)^{6,7}. These problems can be solved by selecting doping HfO_2 material followed by rapid thermal annealing at high temperatures. It was found that, the largest memory window is reached when using La as a dopant⁸. Also, when using $\text{Hf}_{0.5}\text{Zr}_{0.5}\text{O}_2$ instead of HfO_2 , the wake-up effect is suppressed and the annealing temperature decreases⁹, which is compatible with the thermal budget of back-end-of-line. The ferroelectric response of the structure is also influenced by the method of metal contacts deposition and the annealing temperature. The highest memory window value for $\text{Hf}_{0.5}\text{Zr}_{0.5}\text{O}_2$ films without doping was obtained by applying the *in vacuo* process, without atmospheric influence on the structure, which made it possible to obtain a memory window of $2P_r = 54.2 \mu\text{C}/\text{cm}^2$ due to the improvement of the ferroelectric/metal interface quality¹⁰. Recently, it has been discovered that when $\text{Hf}_{0.5}\text{Zr}_{0.5}\text{O}_2$ is doped with La, Y and their mixture, the films remain functional after 10^{11} rewriting cycles, demonstrating quite a large MW value^{11,12}. However, doping with La led to a more pronounced manifestation of the wake-up effect.

The possible reason of this effect might be caused by the influence of metal electrodes. The $\text{Hf}_{0.5}\text{Zr}_{0.5}\text{O}_2$:La-based structures in Refs. 11,12 had both bottom (BE) and top (TE) TiN metal electrodes. Recently, it has been shown that using RuO_2 as the TE in TiN/ $\text{Hf}_{0.5}\text{Zr}_{0.5}\text{O}_2$ / RuO_2 ¹³, as both the TE and the BE in RuO_2 / $\text{Hf}_{0.5}\text{Zr}_{0.5}\text{O}_2$ / RuO_2 ¹⁴ and Ru as the BE in

^{a)}Electronic mail: timz@isp.nsc.ru

TABLE I. Structures of all samples with different BE and TE under study

Sample	Structure	BE	TE
S1	TiN/Hf _{0.5} Zr _{0.5} O ₂ /TiN	TiN	TiN
S2	TiN/Hf _{0.5} Zr _{0.5} O ₂ /RuO _x	TiN	RuO _x
S3	TiN/Hf _{0.5} Zr _{0.5} O ₂ /TiAlN	TiN	TiAlN
S4	TiN/Hf _{0.5} Zr _{0.5} O ₂ /NbN	TiN	NbN
S5	W/Hf _{0.5} Zr _{0.5} O ₂ /TiN	W	TiN
S6	W/Hf _{0.5} Zr _{0.5} O ₂ /W	W	W
S7	TiN/Hf _{0.5} Zr _{0.5} O ₂ /W	TiN	W

Ru/Hf_{0.5}Zr_{0.5}O₂/TiN¹⁵ structures leads to a small memory window value and a relatively early breakdown during the electric field cycling. Other metal electrodes were explored to promote the ferroelectric phase in Hf_{1-x}Zr_xO₂ including TaN^{16,17}, Ir^{18,19}, Pt²⁰⁻²² and W²³ without endurance measurements.

In this letter, we investigate the impact of different metal electrodes of Hf_{0.5}Zr_{0.5}O₂ in metal-ferroelectric-metal structures during the endurance cycling.

The structures under study in this work were metal-1/Hf_{0.5}Zr_{0.5}O₂/metal-2 (M1/FE/M2) ferroelectric capacitors on silicon substrates with the ferroelectric thicknesses of 10 nm. Totally, seven kinds of samples with different electrodes were studied. A description of all samples is provided in Table I. M1/FE/M2 capacitors were fabricated by the following procedure. The 50 nm thick W layer, as well as 10 nm thick TE and BE were deposited on a silicon substrate at room temperature using a sputtering system from Alliance Concept. To produce S5 and S6 samples, the BE deposition step was skipped, *i.e.* Hf_{0.5}Zr_{0.5}O₂ films for these structures were deposited directly on the W layers. The 10 nm thick Hf_{0.5}Zr_{0.5}O₂ films were deposited by atomic layer deposition (ALD) at deposition temperature 280°C in the Oxford Instruments OPAL system. For hafnium and zirconium oxides, tetrakis[ethylmethylamino]hafnium (Hf[N(C₂H₅)CH₃]₄) and tris[dimethylamino]cyclopentadienyl-zirconium (C₅H₅)Zr[N(CH₃)₂]₃) were used as precursors, respectively. H₂O was used as an oxidant for all ALD cycles. The samples were then treated by RTA at 600°C for 20 s in the N₂ atmosphere. To pattern the capacitor structures, a 10 nm thick Ti layer was deposited as an adhesion layer, and then 25 nm thick Pt was deposited by the electron beam evaporation through a shadow mask. The round-shaped metal contact diameter was 200 μm. The wet chemical etching of TE was carried out for patterning using the SC1 etching (5% NH₃ and 2% H₂O₂ solutions in H₂O at the temperature of 50°C). The schematic structures of the samples under study with different BE and TE are shown in Fig. 1. To produce S2, S6 and S7 samples, RuO₂ or W electrodes were deposited by physical vapor deposition through a shadow mask on the Hf_{0.5}Zr_{0.5}O₂ films instead of the upper TiN electrode.

An experimental study of the ferroelectric properties

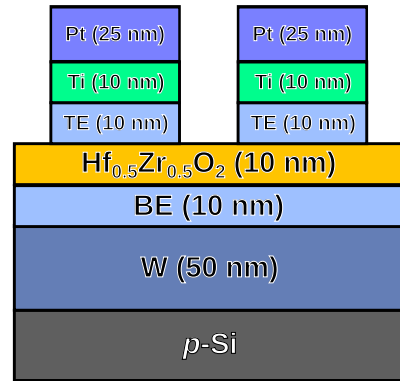


FIG. 1. Schematic structure of the samples under study with different BE and TE.

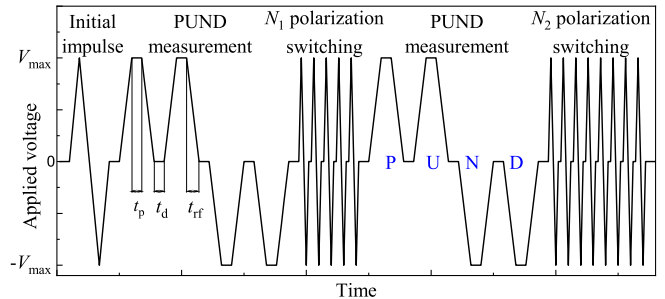


FIG. 2. Schematic voltage sweeps during the endurance measurements at different points. Letters in blue show P, U, N and D pulses of the PUND sequence.

evolution during the structure state switching was carried out by the cyclic application of trapezoidal voltage pulses of positive and negative amplitudes. On some pulses, polarization-voltage (P - V) characteristics were measured by the PUND technique followed by the DC current-voltage (I - V) measurements with the same voltage amplitude. The measurements by the PUND method consist in the sequential application of two positive pulses (Positive/Up) and two negative (Negative/Down) to the structure. The PUND sequences and cyclic voltage pulses are shown in Fig. 2 schematically. The charge-carrier polarization values P_r during the cycling were obtained from the PUND measurements. For the PUND measurements, the voltage rise/fall times t_{rf} , pulse delay t_d and plateau time t_p were the same and amounted 100 μs. The times for the cycling pulses were $t_{rf} = 0.5$ μs, $t_p = 2$ μs and $t_d = 1.0$ μs. The cycling pulse durations ensure that the polarization is switched to at least 80% of the maximum possible value. The voltage of all pulses was 3.0 V, since at this amplitude value a compromise ratio of the memory window and the cycling duration was observed²⁴. The DC measurements were carried out from -0.2 to +3.0 V in 0.1 V increments for 7 sec. Such long voltage sweep duration allows us to reduce the displacement current contributions and to extract their values at zero voltage. The measurements were carried out using a Keithley

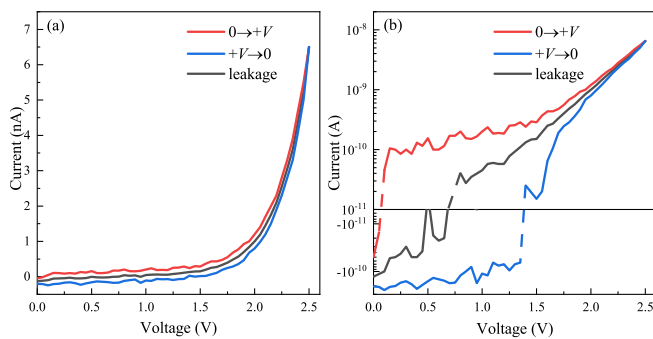


FIG. 3. (a) Currents flowing when the voltage increases $I_{0 \rightarrow +V}(V)$ (red lines) and when the voltage decreases $I_{+V \rightarrow 0}(V)$ (blue line). The displacement currents $\pm C(V)dV/dt$ change sign as the voltage increases and decreases, while the leakage currents $I_{\text{leakage}}(V)$ do not. As a result of averaging the currents of $I_{0 \rightarrow +V}(V)$ and the $I_{+V \rightarrow 0}(V)$, only leakage currents (black lines) remain. (b) The same data in the semilog plate. Dashed lines connect positive and negative current values.

4200-SCS parametric analyzer with 4225-PMU (pulses and PUND) and SMU-4210 (DC) units at room temperature. The experiments were carried out up to the sample break down or when P_r becomes negligible.

Following the PUND method, DC measurements made it possible to obtain leakage currents. As a result of averaging the currents measured during the forward ($0 \rightarrow \pm V$) and reverse ($\pm V \rightarrow 0$) voltage sweep, displacement currents were excluded, and leakage currents were obtained:

$$I_{\text{leakage}}(V) = 1/2 (I_{0 \rightarrow +V}^{\text{DC}}(V) + I_{+V \rightarrow 0}^{\text{DC}}(V)). \quad (1)$$

The procedure for extracting the leakage current is illustrated in Fig. 3. The mean distance between neighboring traps a was extracted from the I - V dependences of the leakage currents within the model of phonon-assisted tunneling of electrons (holes) between neighboring traps (PATENT)²⁵. Recently, it has been demonstrated that this transport model adequately describes the leakages in both amorphous and ferroelectric HfO₂-based films^{26–28} as well as in Hf_{0.5}Zr_{0.5}O₂-based structures^{29–31}. This procedure is described in details elsewhere^{31–33}.

The presence of Hf_{0.5}Zr_{0.5}O₂ film ferroelectric properties is confirmed by observing the hysteresis in the polarization-voltage characteristics for all M1/FE/M2 structures. In Fig. 4 is the evolution of the ferroelectric and transport properties of M1/FE/M2 structures with different bottom and top metal electrodes. The S1 sample with TiN BE and TE exhibits a typical charge-carrier polarization (P_r^\pm) evolution (black characters in Fig. 4(a)) in accordance with literature data^{31,34}: it endures more than 10^6 switch cycles with a slight wake-up and fatigue effects with $MW = |P_r^+| + |P_r^-| \approx 20 \mu\text{C}/\text{cm}^2$ and then breaks down, as shown in Fig. 4 by crosses. The P_r^\pm values for S2 and S3 samples are less than $10 \mu\text{C}/\text{cm}^2$

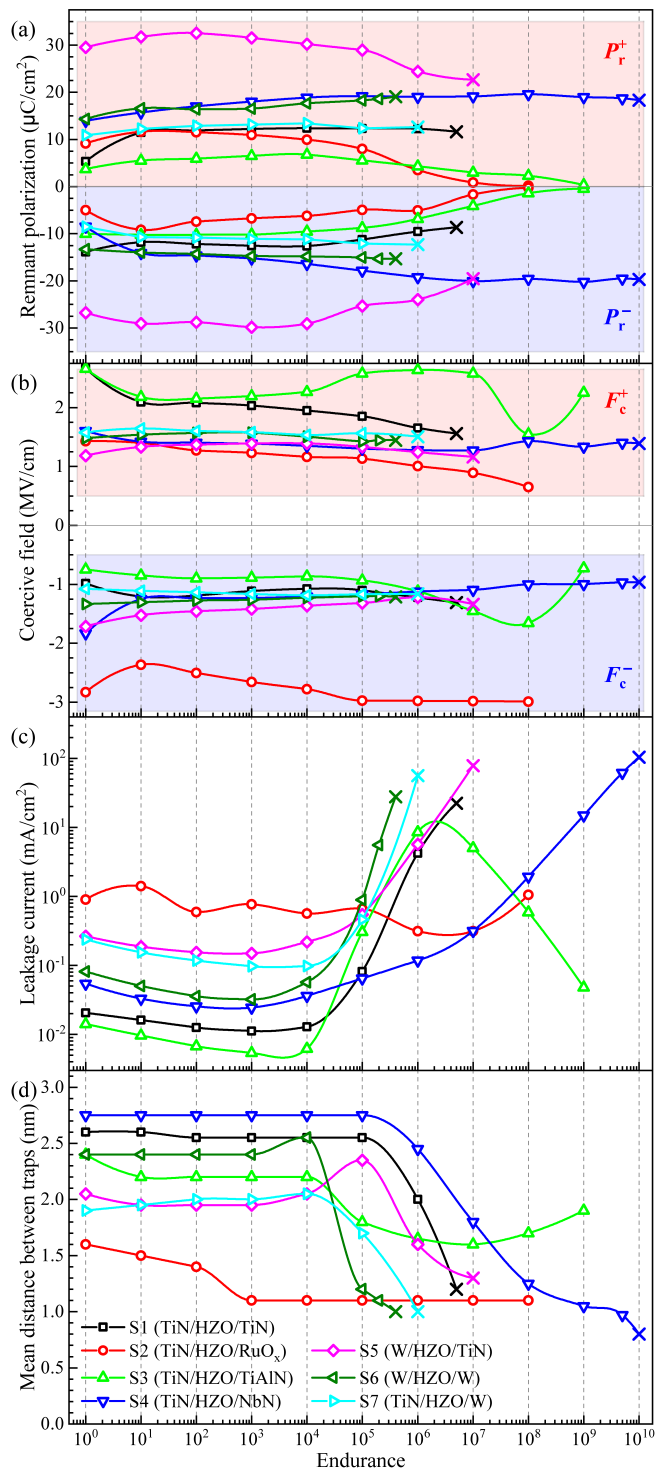


FIG. 4. Evolution of the ferroelectric and transport properties on the M1/FE/M2 structures with different bottom and top electrodes: (a) ferroelectric memory windows, (b) coercive fields, (c) the leakage current values at 3.0 V and (d) the mean distance between traps. Crosses show the last obtained data before breakdown. Vertical dashed lines are visual guides.

and disappear after 10^8 – 10^9 switching cycles. The S5 sample exhibits the largest residual polarization with $MW \approx 60 \mu\text{C}/\text{cm}^2$. After expressive fatigue effect, the sample reaches a breakdown after 10^7 endurance cycles. The MW values for samples S1, S4, S6 and S7 are close, but all of them, except S4, are broken down after 10^5 – 10^7 switch cycles. The sample with NbN TE (S4) endures more than 10^{10} repolarization with $MW \approx 30$ – $40 \mu\text{C}/\text{cm}^2$.

The coercive field values F_c^\pm (Fig. 4(b)) are constant with small deviations for almost all structures under study except for S2 and S3 samples. As far as the MW disappears, F_c^\pm loses its physical meaning. One can see that measured F_c^\pm values exhibit slight asymmetry. This can be caused by built-in electric field due to different work functions of the metal electrodes. Also, asymmetric interfaces around ferroelectric films, due to the exposure of all BEs to the ALD processing temperature, can introduce distortions in the F_c^\pm measurements.

The leakage currents, measured at the voltage of 3 V are shown in Fig. 4(c). One can see that leakages rise after 10^4 cycles for all structures, but the S2 sample, which exhibits constant leakage current. The leakage current of structure S3 shows complex evolution: namely, up to 10^4 endurance cycles, its value decreases, then increases, and after 10^6 cycles it decreases to the original value.

The extracted mean distances between neighboring traps are shown in Fig. 4(d). One can see that the distances between traps in ferroelectrics of almost all structures remain at the same levels up to 10^4 cycles of repolarization. Reducing the average distances between traps after 10^4 – 10^5 switching cycles are accompanied by an increase in leakage currents due to their exponential dependence²⁵.

Since the traps in $\text{Hf}_{0.5}\text{Zr}_{0.5}\text{O}_2$ are oxygen vacancies, a decrease in the distances between traps is associated with new oxygen vacancy generation^{29,31}. Oxygen ions that left the crystal lattice can migrate in an external electric field and even leave the $\text{Hf}_{0.5}\text{Zr}_{0.5}\text{O}_2$ film for a metal electrode³⁵. The S4 structure is formed with the top NbN electrode, i.e., it is more corrosion and oxidation resistant than TiN³⁶. Thus, the TiN electrode in the structures absorbs more oxygen than NbN. This effect leads to a greater endurance of the structure during repolarization even with a large number of defects.

It is difficult to determine where new oxygen vacancies are located. We assume that, initially, there are many traps in the grain boundaries and much less in the grain bulk. Thus, the leakage current is caused by traps at the grain boundaries. After 10^4 cycles new traps are generated in the grain bulk due to the oxygen ion migration during the cyclic switching, and some ions O^- might reach grain boundaries or even the $\text{Hf}_{0.5}\text{Zr}_{0.5}\text{O}_2$ /metal interface followed by the absorption of electrodes. Then the leakage currents are limited by the traps in the grain bulk. In this case, part of the applied voltage drops at the interface layer between $\text{Hf}_{0.5}\text{Zr}_{0.5}\text{O}_2$ and the electrode, such as WO_x for W³⁷ or TiO_N for TiN³⁸. If the traps

are located in the grain boundaries, then the mean distance between the traps a can be converted to the surface (2D) trap density $N_{2D} = a^{-2} \sim 10^{13}$ – 10^{14} cm^{-2} . If the traps are distributed in the grain bulk, then the volumetric (3D) trap density is $N_{3D} = a^{-3} \sim 10^{19}$ – 10^{21} cm^{-3} .

It is interesting to note that the S5 structure with W BE exhibits an extremely high MW value, compared to other structures. We assume that this is caused by the absence of the interface sublayer WO_x with high static dielectric constant after the $\text{Hf}_{0.5}\text{Zr}_{0.5}\text{O}_2$ deposition. This is confirmed by the HAXPES analysis conducted for the same set of structures³⁷. The endurance cycling leads to a fast generation of new oxygen vacancies in $\text{Hf}_{0.5}\text{Zr}_{0.5}\text{O}_2$, forming the sub-layer followed by a breakdown. RuO_x and TiAlN electrodes absorb oxygen more actively than other metals, the interface sublayer is formed faster, and the voltage drops on it³⁹. This leads to the vanishing of the ferroelectric response in $\text{Hf}_{0.5}\text{Zr}_{0.5}\text{O}_2$ films and decrease in leakage currents. It should be noted that these samples were not broken down. One can assume that RuO_x and TiAlN electrodes are good for the DRAM application.

Also, it is interesting to note that S5 and S7 structures are symmetrical to each other, but exhibit their different ferroelectric evolution during the endurance procedure. We assume that this is caused by different temperature influences on the BE (280°C) and the TE (room temperature) during the ferroelectric film deposition and formation the structure as a whole. It should be noted that not only the electrode material, but also its specific properties such as grain texture can affect the $\text{Hf}_{0.5}\text{Zr}_{0.5}\text{O}_2$ film properties and performance. The study of the metal electrodes structural properties and their effect on the $\text{Hf}_{0.5}\text{Zr}_{0.5}\text{O}_2$ film ferroelectric properties is beyond the scope of this work and is a task for the future.

In conclusion, transport experiments, combined with simulations, were studied for thin $\text{Hf}_{0.5}\text{Zr}_{0.5}\text{O}_2$ ferroelectric film-based structures with different metal electrodes. It was found that RuO_x and TiAlN electrodes suppress the ferroelectric response in $\text{Hf}_{0.5}\text{Zr}_{0.5}\text{O}_2$ films, as well as leakages through the structure. The utilization of NbN as an electrode in M/FE/M structures allows obtaining a more stable ferroelectric capacitor with more than 10^{10} cycle switches.

ACKNOWLEDGMENTS

The work was performed within the framework of the state assignment of the Ministry of Education and Science of the Russian Federation for the Rzhanov Institute of Semiconductor Physics of the Siberian Branch of the Russian Academy of Sciences. The authors would like to express their gratitude to Prof. Thomas Mikolajick, Dr. Uwe Schroeder, Ruben Alcalá and Monica Materano for the provided samples. The authors would like to acknowledge and thank Dr. Uwe Schroeder and Dr. Alexey Mironov for their valuable discussions.

CONFLICT OF INTEREST

The authors have no conflicts to disclose.

DATA AVAILABILITY

The data that support the findings of this study are available from the corresponding author upon reasonable request.

- ¹D. Bondurant, *Ferroelectrics* **112**, 273 (1990).
- ²T. S. Böске, J. Müller, D. Bräuhaus, U. Schröder, and U. Böttger, *Applied Physics Letters* **99**, 102903 (2011).
- ³T. S. Böске, S. Teichert, D. Bräuhaus, J. Müller, U. Schröder, U. Böttger, and T. Mikolajick, *Applied Physics Letters* **99**, 112904 (2011).
- ⁴X. Sang, E. D. Grimley, T. Schenk, U. Schroeder, and J. M. LeBeau, *Applied Physics Letters* **106**, 162905 (2015).
- ⁵M. Trentzsch, S. Flachowsky, R. Richter, J. Paul, B. Reimer, D. Utess, S. Jansen, H. Mulaosmanovic, S. Muller, S. Slesazek, J. Ocker, M. Noack, J. Muller, P. Polakowski, J. Schreiter, S. Beyer, T. Mikolajick, and B. Rice, in *2016 IEEE International Electron Devices Meeting (IEDM)* (IEEE, 2016) pp. 11.5.1–11.5.4.
- ⁶S. Mueller, J. Muller, U. Schroeder, and T. Mikolajick, *IEEE Trans. Device Mater. Rel.* **13**, 93 (2013).
- ⁷M. Pesić, F. P. G. Fengler, S. Slesazek, U. Schroeder, T. Mikolajick, L. Larcher, and A. Padovani, in *2016 IEEE International Reliability Physics Symposium (IRPS)* (IEEE, 2016) pp. MY-3-1–MY-3-5.
- ⁸U. Schroeder, E. Yurchuk, J. Müller, D. Martin, T. Schenk, P. Polakowski, C. Adelman, M. I. Popovici, S. V. Kalinin, and T. Mikolajick, *Japanese Journal of Applied Physics* **53**, 08LE02 (2014).
- ⁹H. J. Kim, M. H. Park, Y. J. Kim, Y. H. Lee, T. Moon, K. D. Kim, S. D. Hyun, and C. S. Hwang, *Nanoscale* **8**, 1383 (2016).
- ¹⁰Y. Lee, H. Alex Hsain, S. S. Fields, S. T. Jaszewski, M. D. Horgan, P. G. Edgington, J. F. Ihlefeld, G. N. Parsons, and J. L. Jones, *Applied Physics Letters* **118**, 012903 (2021).
- ¹¹M. G. Kozodaev, A. G. Chernikova, E. V. Korostylev, M. H. Park, R. R. Khakimov, C. S. Hwang, and A. M. Markeev, *Journal of Applied Physics* **125**, 034101 (2019).
- ¹²M. I. Popovici, A. M. Walke, J. Bizindavyi, J. Meerschaert, K. Banerjee, G. Potoms, K. Katcko, G. Van den Bosch, R. Delhougne, G. S. Kar, and J. Van Houtdt, *ACS Applied Electronic Materials* **4**, 1823 (2022).
- ¹³M. H. Park, H. J. Kim, Y. J. Kim, W. Jeon, T. Moon, and C. S. Hwang, *physica status solidi (RRL) — Rapid Research Letters* **8**, 532 (2014).
- ¹⁴S. S. Fields, S. W. Smith, S. T. Jaszewski, T. Mimura, D. A. Dickie, G. Esteves, M. David Henry, S. L. Wolfley, P. S. Davids, and J. F. Ihlefeld, *Journal of Applied Physics* **130**, 134101 (2021).
- ¹⁵A. G. Chernikova, M. G. Kozodaev, R. R. Khakimov, S. N. Polyakov, and A. M. Markeev, *Applied Physics Letters* **117**, 192902 (2020).
- ¹⁶S. Migita, H. Ota, H. Yamada, K. Shibuya, A. Sawa, and A. Toriumi, *Japanese Journal of Applied Physics* **57**, 04FB01 (2018).
- ¹⁷S. W. Smith, A. R. Kitahara, M. A. Rodriguez, M. D. Henry, M. T. Brumbach, and J. F. Ihlefeld, *Applied Physics Letters* **110**, 072901 (2017).
- ¹⁸M. H. Park, H. J. Kim, Y. J. Kim, W. Lee, T. Moon, K. D. Kim, and C. S. Hwang, *Applied Physics Letters* **105**, 072902 (2014).
- ¹⁹T. Shimizu, T. Yokouchi, T. Shiraishi, T. Oikawa, P. S. S. R. Krishnan, and H. Funakubo, *Japanese Journal of Applied Physics* **53**, 09PA04 (2014).
- ²⁰M. H. Park, H. J. Kim, Y. J. Kim, W. Lee, H. K. Kim, and C. S. Hwang, *Applied Physics Letters* **102**, 112914 (2013).
- ²¹M. H. Park, H. J. Kim, Y. J. Kim, T. Moon, and C. S. Hwang, *Applied Physics Letters* **104**, 072901 (2014).
- ²²T. Shimizu, T. Yokouchi, T. Oikawa, T. Shiraishi, T. Kiguchi, A. Akama, T. J. Konno, A. Gruverman, and H. Funakubo, *Applied Physics Letters* **106**, 112904 (2015).
- ²³G. Karbasian, R. dos Reis, A. K. Yadav, A. J. Tan, C. Hu, and S. Salahuddin, *Applied Physics Letters* **111**, 022907 (2017).
- ²⁴T. M. Zalyalov and D. R. Islamov, in *2022 IEEE 23rd International Conference of Young Professionals in Electron Devices and Materials (EDM)*, IEEE (IEEE, 2022) pp. 48–51.
- ²⁵K. A. Nasyrov and V. A. Gritsenko, *JETP* **112**, 1026 (2011).
- ²⁶D. R. Islamov, V. A. Gritsenko, C. H. Cheng, and A. Chin, *Applied Physics Letters* **105**, 222901 (2014), arXiv:1409.6887 [cond-mat.mtrl-sci].
- ²⁷V. A. Gritsenko, T. V. Perevalov, and D. R. Islamov, *Physics Reports* **613**, 1 (2016).
- ²⁸V. A. Gritsenko and A. A. Gismatulin, *Applied Physics Letters* **117**, 142901 (2020).
- ²⁹D. R. Islamov, T. V. Perevalov, V. A. Gritsenko, C. H. Cheng, and A. Chin, *Applied Physics Letters* **106**, 102906 (2015), arXiv:1501.02370 [cond-mat.mtrl-sci].
- ³⁰D. R. Islamov, A. G. Chernikova, M. G. Kozodaev, A. M. Markeev, T. V. Perevalov, V. A. Gritsenko, and O. M. Orlov, *JETP Letters* **102**, 544 (2015).
- ³¹D. R. Islamov, V. A. Gritsenko, T. V. Perevalov, V. A. Pustovarov, O. M. Orlov, A. G. Chernikova, A. M. Markeev, S. Slesazek, U. Schroeder, T. Mikolajick, and G. Y. Krasnikov, *Acta Materialia* **166**, 47 (2019).
- ³²D. R. Islamov, V. A. Gritsenko, and A. Chin, *Optoelectronics, Instrumentation and Data Processing* **53**, 184 (2017).
- ³³A. A. Pil'nik, A. A. Chernov, and D. R. Islamov, *Scientific Reports* **10**, 15759 (2020).
- ³⁴J. Müller, T. S. Böске, D. Bräuhaus, U. Schröder, U. Böttger, J. Sundqvist, P. Kücher, T. Mikolajick, and L. Frey, *Applied Physics Letters* **99**, 112901 (2011).
- ³⁵P. Nukala, M. Ahmadi, Y. Wei, S. de Graaf, E. Stylianidis, T. Chakraborty, S. Matzen, H. W. Zandbergen, A. Björling, D. Mannix, D. Carbone, B. Kooi, and B. Noheda, *Science* **372**, 630 (2021).
- ³⁶H. C. Barshilia, M. S. Prakash, A. Poojari, and K. S. Rajam, *Thin Solid Films* **460**, 133 (2004).
- ³⁷R. Alcalá, M. Materano, P. D. Lomenzo, P. Vishnumurthy, W. Hamouda, C. Dubourdieu, A. Kersch, N. Barrett, T. Mikolajick, and U. Schroeder, *Advanced Functional Materials* **33**, 2303261 (2023).
- ³⁸E. D. Grimley, T. Schenk, X. Sang, M. Pesić, U. Schroeder, T. Mikolajick, and J. M. LeBeau, *Advanced Electronic Materials* **2**, 1600173 (2016).
- ³⁹R. Alcalá, F. Mehmood, P. Vishnumurthy, T. Mittmann, T. Mikolajick, and U. Schroeder, in *2022 IEEE International Memory Workshop (IMW)* (IEEE, 2022).